Supplementary Information

Metal chalcogenide electron extraction layers for *nip*-type tin-based perovskite solar cells

Tianpeng Li[1,†], Bin Li[2,†], Yingguo Yang[3,4], Zuoming Jin[1], Zhiguo Zhang[1], Peilin Wang[1], Liangliang Deng[5], Yiqiang Zhan[5], Qinghong Zhang[2], Jia Liang[1,*]

[1] Department of Materials Science and State Key Laboratory of Photovoltaic Science and Technology, Fudan University, 220 Handan Road, Shanghai 200433, China

[2] State Key Laboratory for Modification of Chemical Fibers and Polymer Materials, College of Materials Science and Engineering, Donghua University, Shanghai 201620, China

[3] School of Microelectronics, Fudan University, 220 Handan Road, Shanghai, 200433 China

[4] Shanghai Synchrotron Radiation Facility (SSRF), Shanghai Advanced Research Institute, Chinese Academy of Sciences, Shanghai, 201800 China

[5] Center of Micro-Nano System, School of Information Science and Technology, Fudan University, 220 Handan Road, Shanghai 200433, China

[†] These authors contributed equally: Tianpeng Li, Bin Li.

* Email: jialiang@fudan.edu.cn

Contents

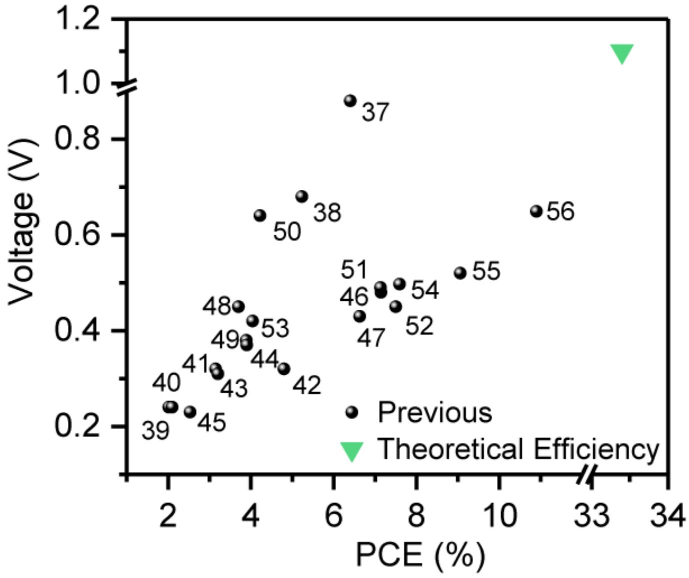

Supplementary Fig. 1. Comparison between theorectical and experimental results. Statistics of the recently reported V_{OC} and PCE of *nip*-type TPSCs. The theorectical values were also listed here for comparison.

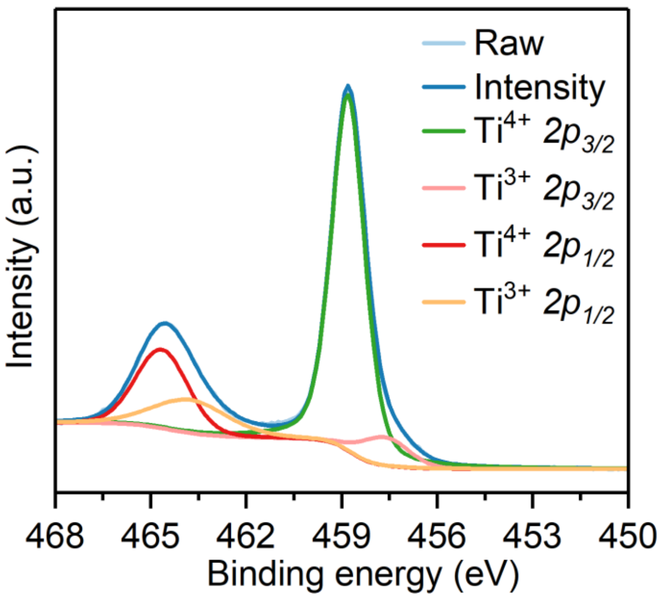

Supplementary Fig. 2. XPS spectra. High-resolution XPS sepctum in the Ti 2p region of the TiO_2 ETL.

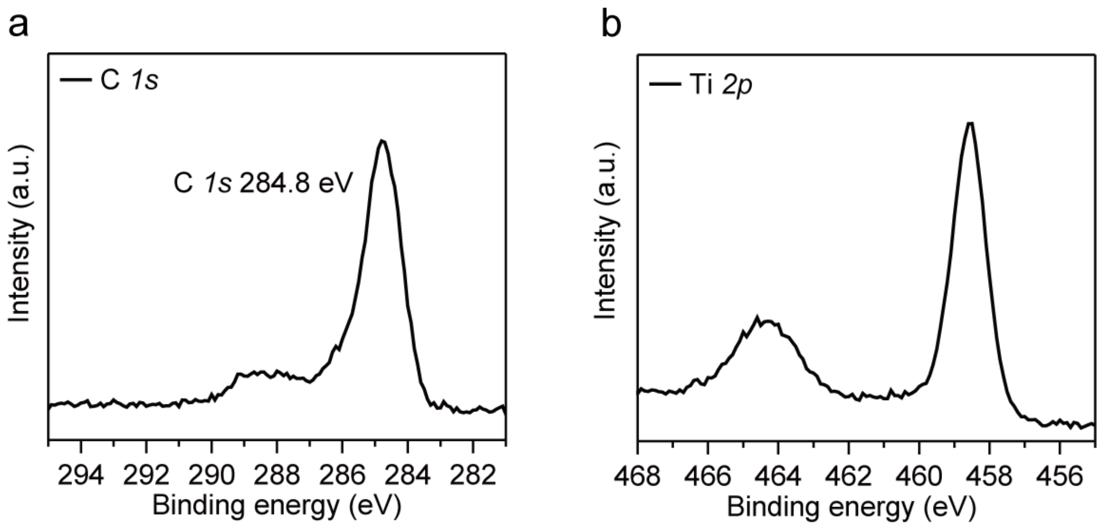

Supplementary Fig. **3**. **XPS spectra**. High-resolution XPS spectra in the **a**, C 1s and **b**, Ti 2p regions of the Sn-based perovskite films deposited on the TiO_2 ETL. The concentration of presursor solution of the Sn-based perovskite is 0.1 M.

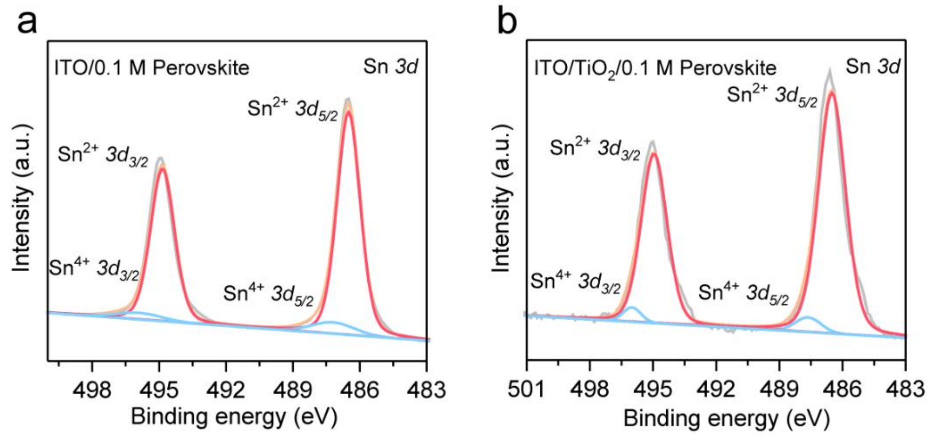

Supplementary Fig. 4. XPS spectra. High-resolution XPS spectra in the Sn 3d region of fresh Sn-based perovskite layers deposited on **a**, ITO and **b**, ITO/TiO_2 substrates.

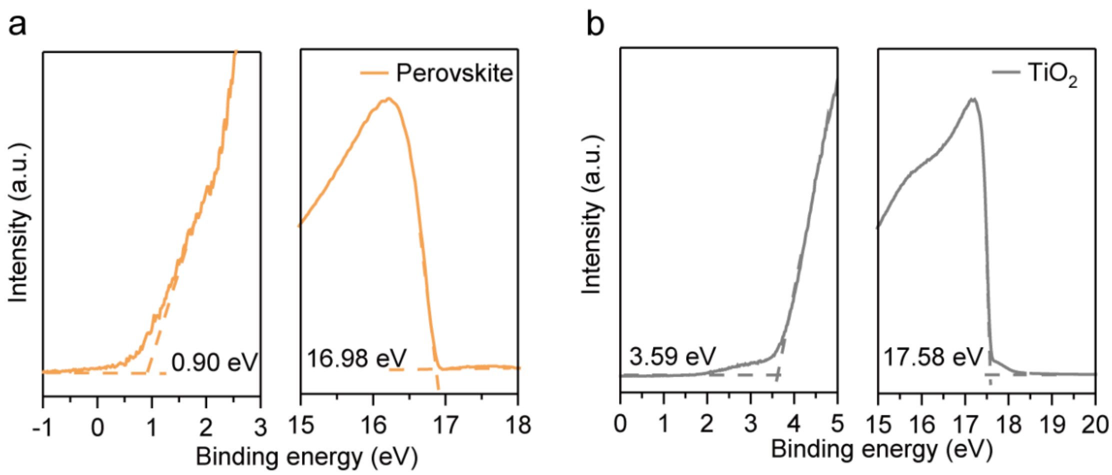

Supplementary Fig. 5. UPS spectra. UPS spectra of VBM onset and photoemission cutoff energy boundary of **a**, Sn-based perovskites and **b**, TiO_2 ETLs.

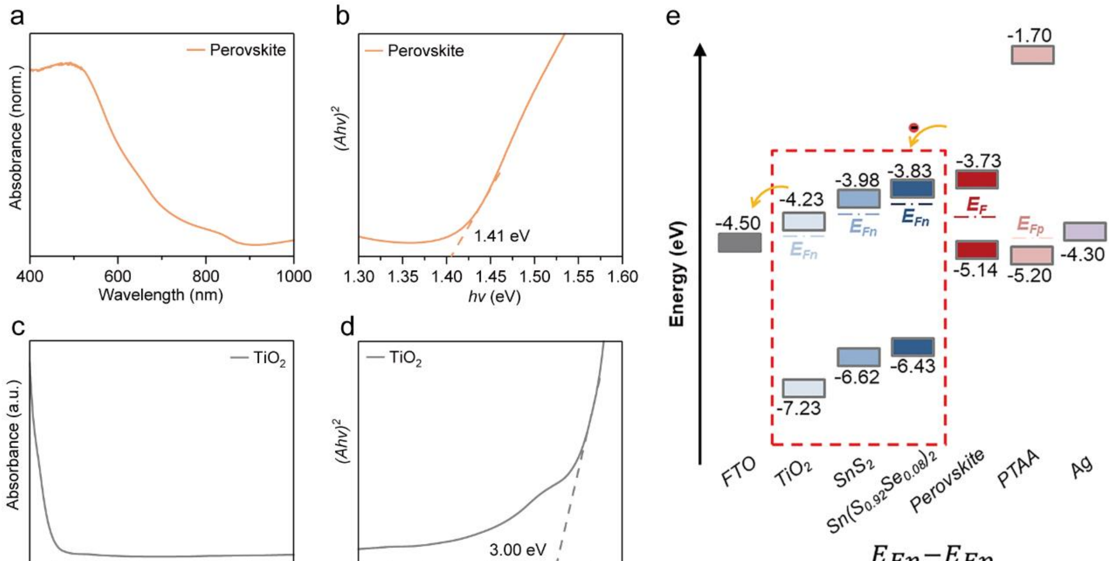

$$V_{OC} = \frac{E_{Fn} - E_{Fp}}{q}$$

Supplementary Fig. 6. UV-vis absorption spectra. UV–vis absorption spectra of **a**, the perovskite layer and **c**, the TiO_2 ETL. The tauc plots of **b**, the perovskite layer and **d**, the TiO_2 ETL derived from the corresponding UV-vis absorption spectra. **e**, Energy level diagram of the *nip*-type TPSCs with the structure of FTO/ETL/Sn-based perovskite/PTAA/Ag, utilizing TiO_2, SnS_2, and $Sn(S_{0.92}Se_{0.08})_2$ films as ETLs, which shows the maximum attainable photovoltage is determined by the quasi-Fermi level splitting of the ETL and hole-transport layer (HTL).

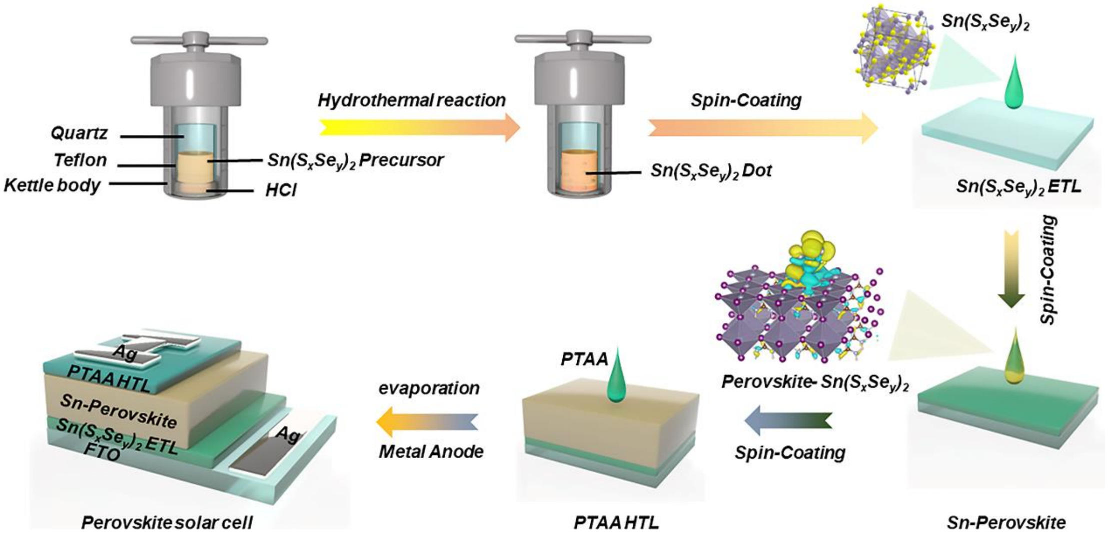

Supplementary Fig. 7. Fabrication process. Schematic diagram of the synthetic process of the metal mixed-chalcogenide ETL ($Sn(S_xSe_y)_2$) and the fabrication process of the corresponding *nip*-type TPSCs.

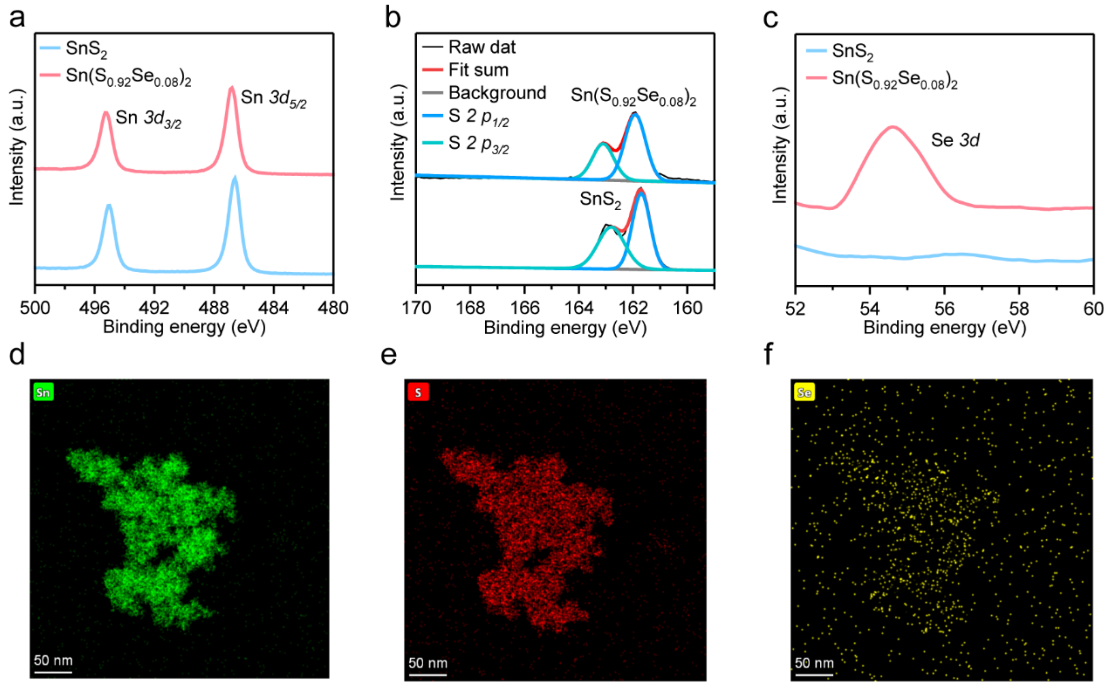

Supplementary Fig. 8. Compositions of metal chalcogenide ETLs. High resolution XPS spectra of the metal chalcogenide ETLs (SnS_2 and $Sn(S_{0.92}Se_{0.08})_2$) in the **a**, Sn 3d, **b**, S 2P, and **c**, Se 3d regions. Transmission electron microscope (TEM) energy dispersive X-ray spectroscopy (EDS) elemental mapping images of **d**, Sn, **e**, S, and **f**, Se elements in the $Sn(S_{0.92}Se_{0.08})_2$ ETL.

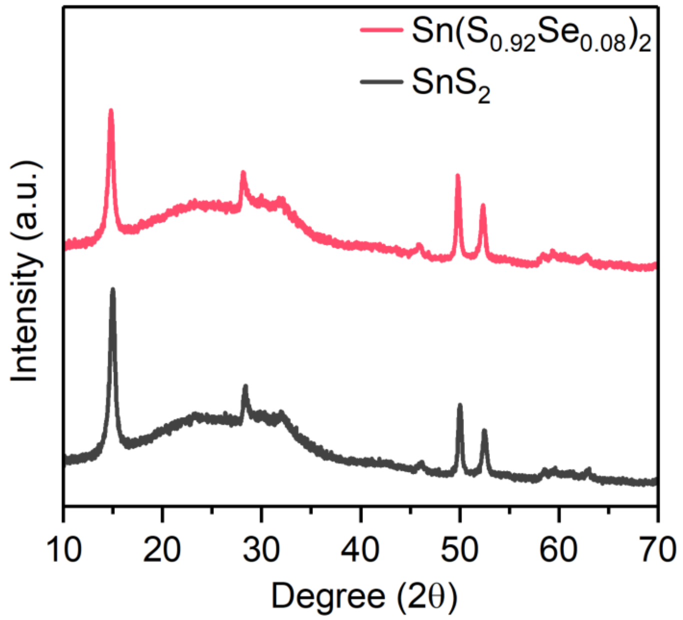

Supplementary Fig. 9. XRD patterns. Typical XRD patterns of SnS_2 and $Sn(S_{0.92}Se_{0.08})_2$ ETLs.

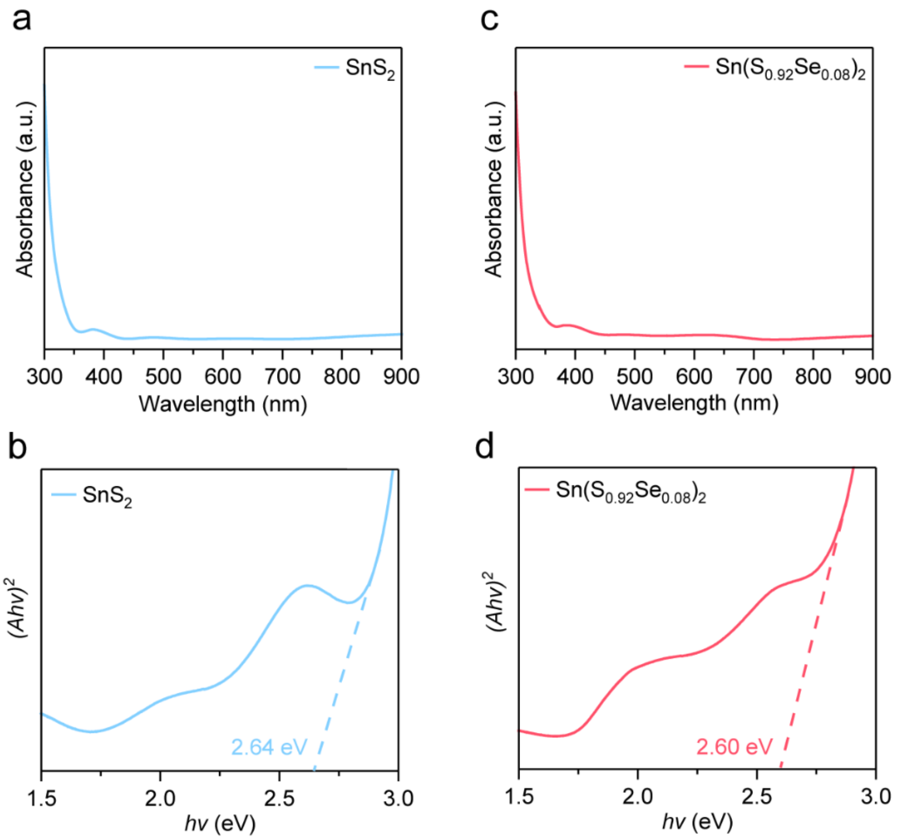

Supplementary Fig. 10. UV-vis absorption spectra of metal chalcogenide ETLs. UV–vis absorption spectra of **a**, the SnS_2 ETL and **c**, the $Sn(S_{0.92}Se_{0.08})_2$ ETL. The tauc plots of **b**, the SnS_2 ETL and **d**, the $Sn(S_{0.92}Se_{0.08})_2$ ETL derived from the corresponding UV-vis absorption spectra.

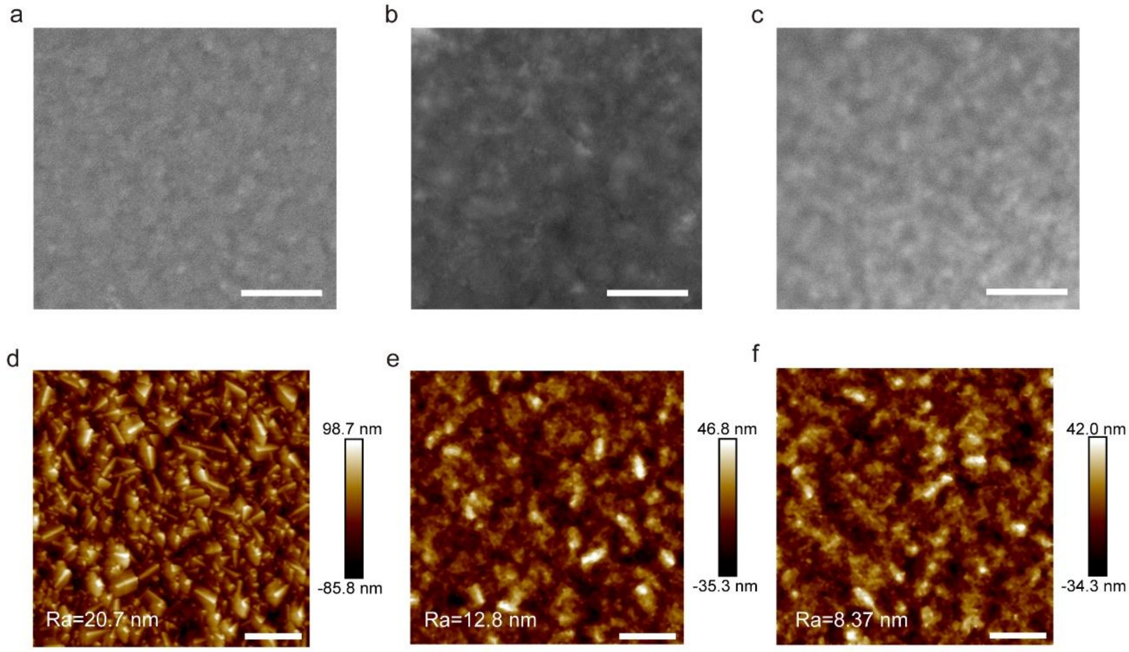

Supplementary Fig. 11. Morphologies of metal chalcogenide ETLs. Top-view SEM images of **a**, TiO_2, **b**, SnS_2 and **c**, $Sn(S_{0.92}Se_{0.08})_2$ ETLs. The scalebars are 500 nm. AFM images of **d**, TiO_2, **e**, SnS_2 and **f**, $Sn(S_{0.92}Se_{0.08})_2$ ETLs. The scalebars are 1 um.

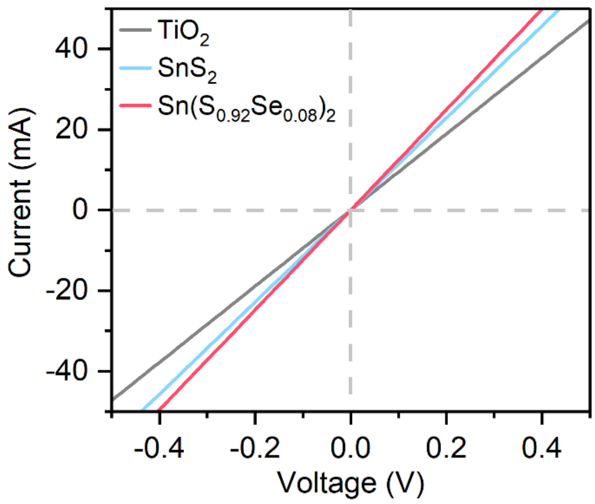

Supplementary Fig. 12. Conductivities of metal chalcogenide ETLs. *I*–*V* characteristics of the TiO_2, SnS_2 and $Sn(S_{0.92}Se_{0.08})_2$ ETLs. The $Sn(S_{0.92}Se_{0.08})_2$ ETL reveals the highest conductivity of 13.8×10^{-3} S cm^{-1} among the three types of ETLs.

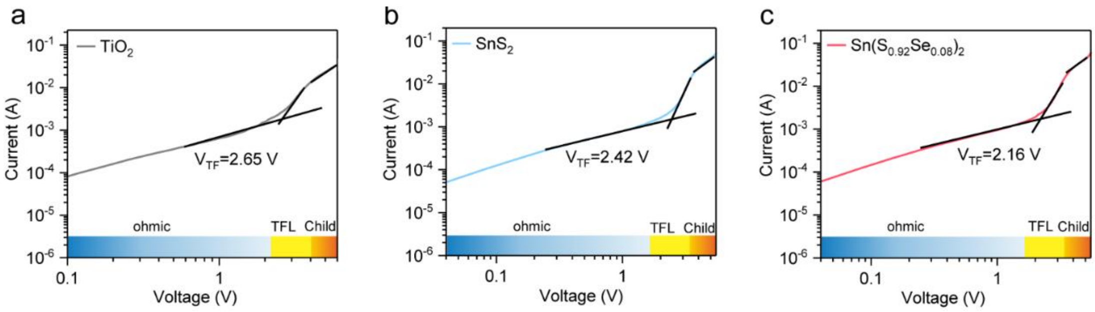

Supplementary Fig. 13. Mobilities of metal chalcogenide ETLs. SCLC spectra of the device with the structure of FTO/Ag/ETL/Ag, the ETLs are **a**, TiO_2, **b**, SnS_2 and **c**, $Sn(S_{0.92}Se_{0.08})_2$ films respectively.

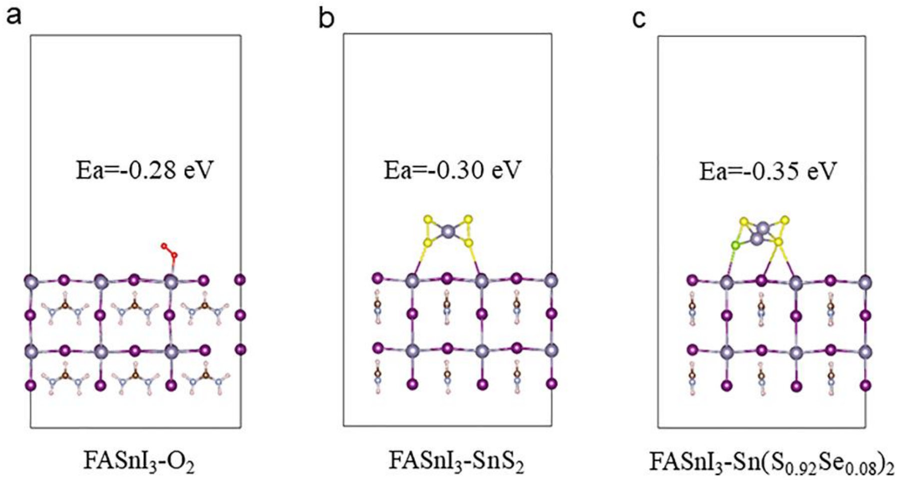

Supplementary Fig. 14. DFT results. The adsorption energy of the Sn-based perovskites reacting with **a**, O_2, **b**, SnS_2 and **c**, $Sn(S_{0.92}Se_{0.08})_2$ molecules, respectively.

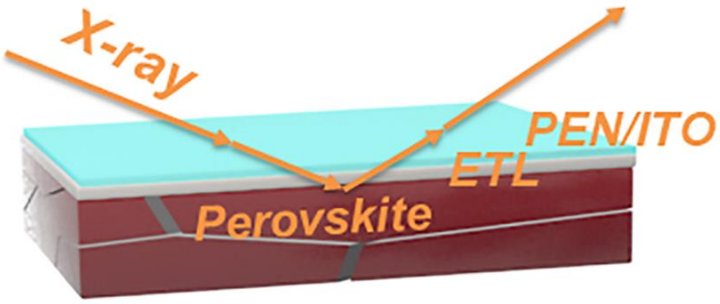

Supplementary Fig. 15. Schematic diagram of the testing mode of illuminating from the back side of the Sn-based perovskite films deposited on PEN/ITO/ETL substrates.

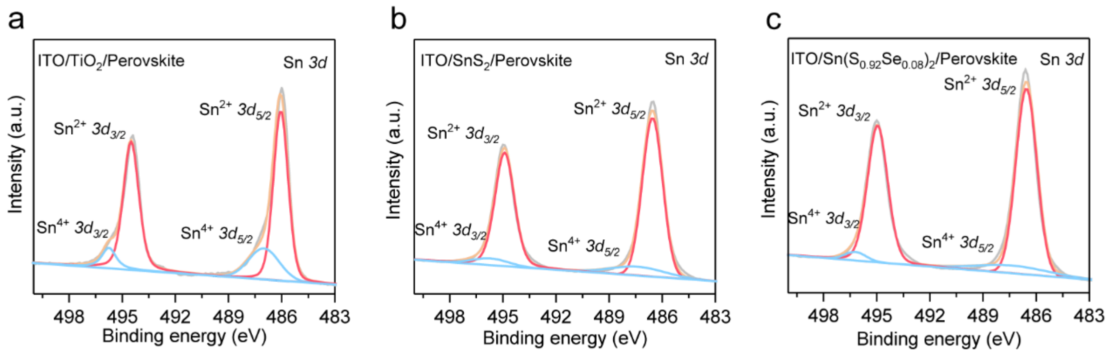

Supplementary Fig. 16. XPS spectra. High-resolution XPS spectra in Sn 3d regions of 2 weeks-aged Sn-based perovskite films deposited on different ETLs, including **a**, TiO_2, **b**, SnS_2 and **c**, $Sn(S_{0.92}Se_{0.08})_2$ ETLs.

Test and Calibration Center of New Energy Device and Module,
Shanghai Institute of Microsystem and Information Technology,
Chinese Academy of Sciences (SIMIT)

中国认可
国际互认
检测
TESTING
CNAS L8490

230017163974

Measurement Report

Report No. 23TR101301

Client Name	Fudan University
Client Address	Handan Rd.220, 200433, Shanghai, China
Sample	Se-SnS_2/Sn perovskite solar cell
Manufacturer	FDU, Jia Liang Group
Measurement Date	13th October, 2023

Performed by:	Qiang Shi *Qiang Shi*	**Date:** 13/10/2023
Reviewed by:	Wenjie Zhao *Wenjie Zhao*	**Date:** 13/10/2023
Approved by:	Yucheng Liu *Yucheng Liu*	**Date:** 13/10/2023

Address: No.235 Chengbei Road, Jiading, Shanghai **Post Code:**201800

E-mail: solarcell@mail.sim.ac.cn **Tel:** +86-021-69976921

1 / 3

137

Report No. 23TR101301

Sample Information	
Sample Type	Se-SnS_2/Sn perovskite solar cell
Serial No.	Se-SnS2-1#
Lab Internal No.	23101301-1#
Measurement Item	I-V characteristic
Measurement Environment	24.8±2.0°C,46.9±5.0%RH

Measurement of I-V characteristic	
Reference cell	PVM 1121
Reference cell Type	mono-Si, WPVS, calibrated by NREL (Certificate No. ISO 2075)
Calibration Value/Date of Calibration for Reference cell	144.53mA/ Feb. 2023
Measurement Conditions	Standard Test Condition (STC): Spectral Distribution: AM1.5 according to IEC 60904-3 Ed.3, Irradiance: 1000±50W/m², Temperature: 25±2℃
Measurement Equipment/ Date of Calibration	AAA Steady State Solar Simulator (YSS-T155-2M) / July.2023 IV test system (ADCMT 6246) / June. 2023 SR Measurement system (CEP-25ML-CAS) / April.2023 Measuring Microscope (MF-B2017C) / July.2023
Measurement Method	I-V Measurement: Logarithmic sweep in both directions (Isc to Voc and Voc to Isc) during one flash based on IEC 60904-1:2020; Spectral Mismatch factor was calculated according to IEC60904-7 and I-V correction according to IEC 60891;
Measurement Uncertainty	Area: 1.0%(k=2); Isc: 1.9%(k=2); Voc: 1.0%(k=2); Pmax: 2.3%(k=2); Eff: 2.5%(k=2)

2 / 3

138

Report No. 23TR101301

====Measurement Results ====

	Forward Scan (Isc to Voc)	Reverse Scan (Voc to Isc)
Area	3.98 mm²	
Isc	0.805 mA	0.811 mA
Voc	0.709 V	0.702 V
Pmax	0.404 mW	0.421 mW
Ipm	0.700 mA	0.737 mA
Vpm	0.576 V	0.571 V
FF	70.74 %	73.94 %
Eff	10.14 %	10.57 %

- Spectral Mismatch Factor: SMM=0.9938.
- Designated illumination area defined by a thin metal mask was measured by measuring microscope.
- Test results listed in this measurement report refer exclusively to the mentioned measured sample.
- The results apply only at the time of the test, and do not imply future performance.

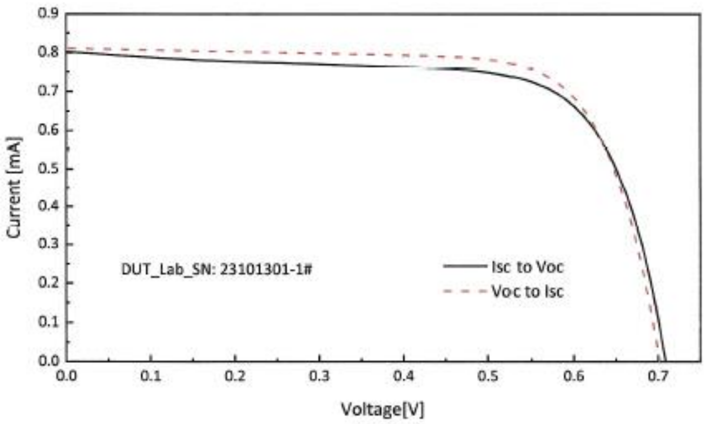

Fig.1 I-V curves of the measured sample

-------End of Report-------

3 / 3

Supplementary Fig. 17. Photovoltaic performance. Certified performance of the nip-type TPSC with the $Sn(S_{0.92}Se_{0.08})_2$ ETL. The certified efficiency is 10.57% under reverse scannign mode with short-circuit current (I_{SC}) = 0.81 mA, V_{OC} = 0.70 V and FF = 73.94%.

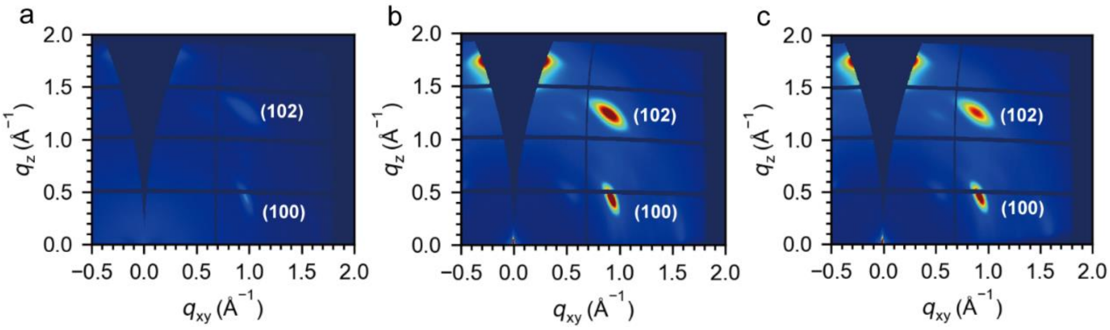

Supplementary Fig. 18. GIWAXS characterization. GIWAXS patterns of Sn-based perovskite layers grown on **a**, TiO_2, **b**, SnS_2, and **c**, $Sn(S_{0.92}Se_{0.08})_2$ ETLs.

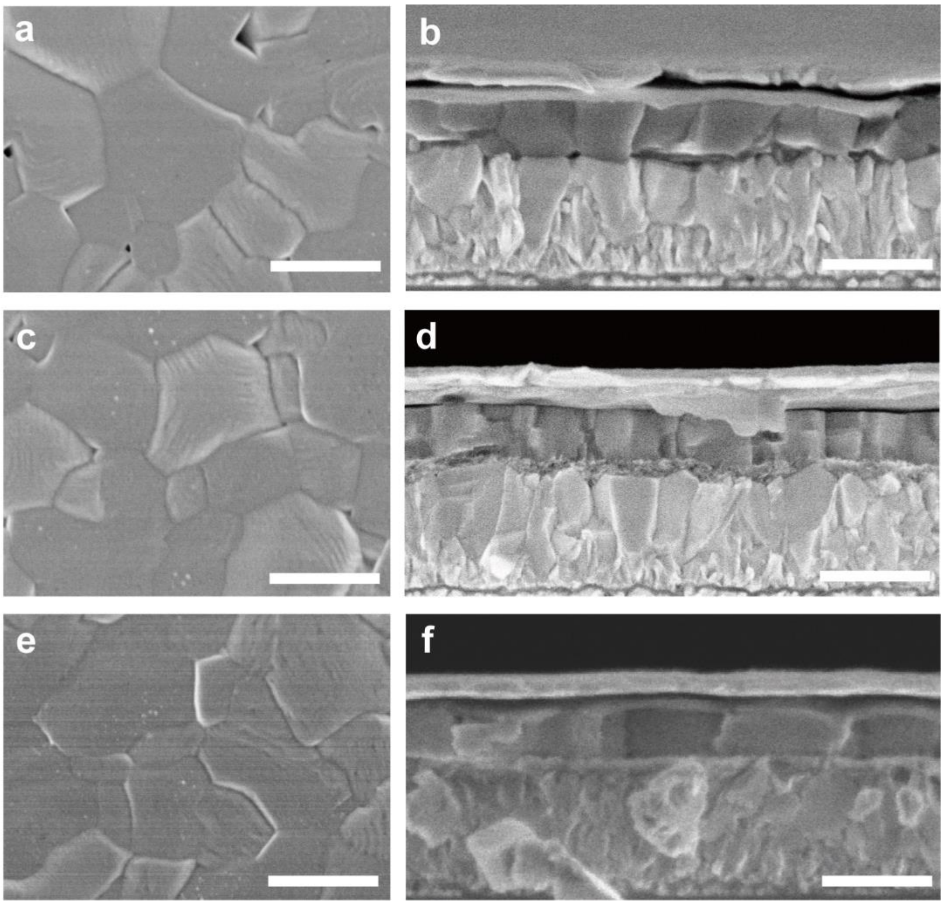

Supplementary Fig. 19. SEM characterizations. Top-view SEM images of the perovskite based on **a**, TiO_2, **c**, SnS_2, and **e**, $Sn(S_{0.92}Se_{0.08})_2$ ETLs. The scalebars are 500 nm. Cross-sectional SEM images of *nip*-type TPSCs with **b**, TiO_2, **d**, SnS_2, and **f**, $Sn(S_{0.92}Se_{0.08})_2$ ETLs. The scalebars are 500 nm.

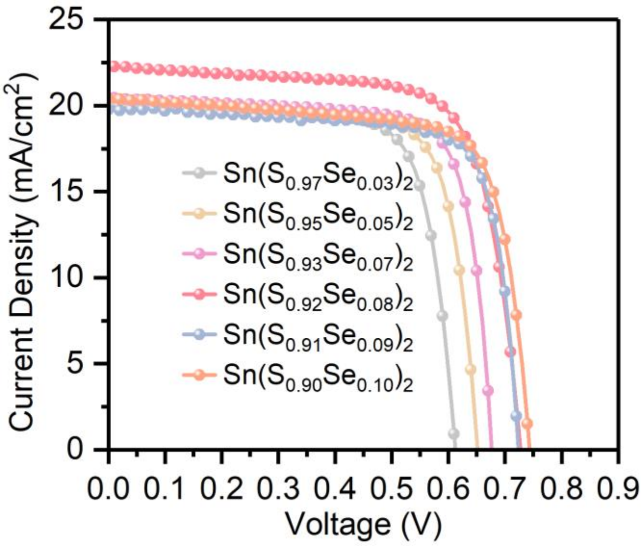

Supplementary Fig. 20. Photovoltaic performances. Photovoltaic performance of the *nip*-type TPSCs based on $Sn(S_xSe_y)_2$ (x+y=1, y = 0.03, 0.05, 0.07, 0.08, 0.09, and 0.10). With the increase of the concentration of Se, the PCEs increased first and then decreased and the *nip*-type TPSC with the $Sn(S_{0.92}Se_{0.08})_2$ ETL shows the best performance.

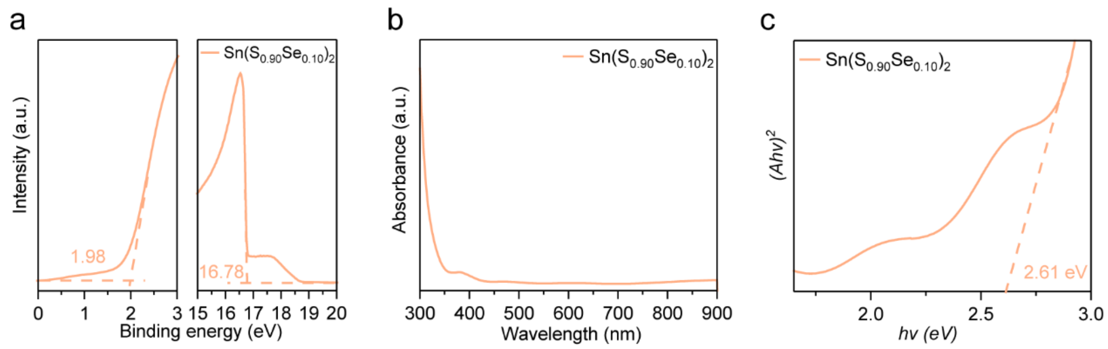

Supplementary Fig. 21. UPS and UV-vis absorption spectra of the $Sn(S_{0.90}Se_{0.10})_2$ ETL. a, UPS spectra, **b,** UV–vis absorption spectra, and **c,** Tauc plot of the $Sn(S_{0.90}Se_{0.10})_2$ ETL.

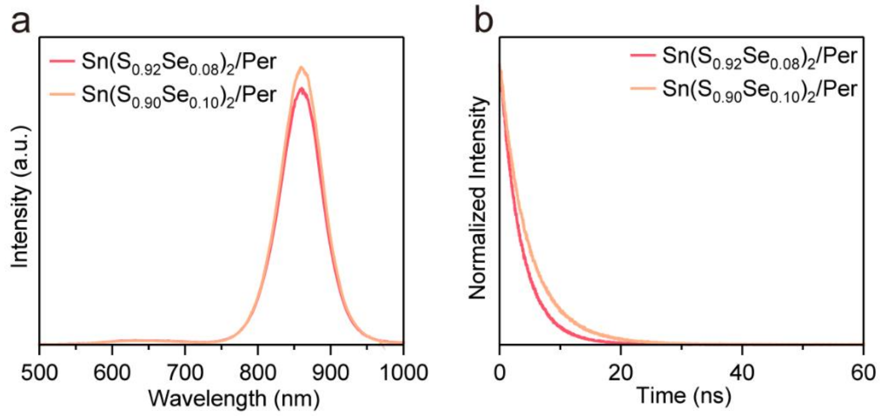

Supplementary Fig. 22. PL and TRPL spectra. a, PL and **b,** TRPL spectra of Sn-based perovskite films deposited on $Sn(S_{0.92}Se_{0.08})_2$ ETLs and $Sn(S_{0.90}Se_{0.10})_2$ ETLs, respectively. These results indicate more pronounced nonradiative interfacial recombination between the Sn-based perovskite layer and the $Sn(S_{0.90}Se_{0.10})_2$ ETL, which suggests faster electron transfer in the structure of Sn-based perovskite films deposited on $Sn(S_{0.92}Se_{0.08})_2$ films.

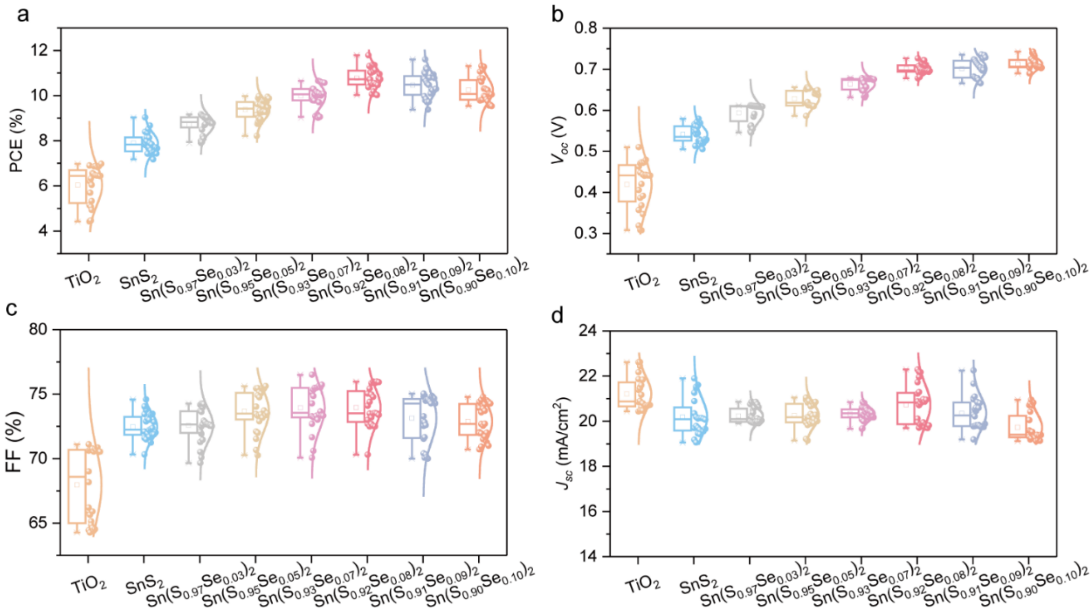

Supplementary Fig. 23. Photovoltaic performance. The statistics of photovoltaic parameters of *nip*-type TPSCs, including **a**, PCE, **b**, V_{OC}, **c**, FF, and **d**, J_{SC}.

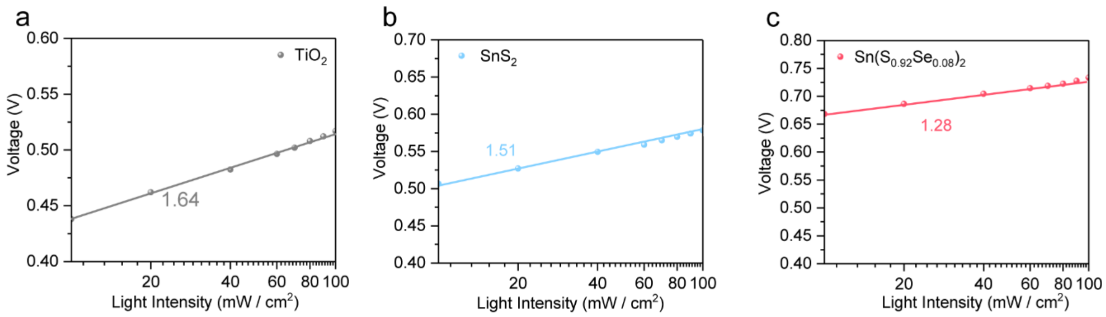

Supplementary Fig. 24. Linear relationship of V_{OC} to the light intensity of the *nip*-type TPSCs with **a**, TiO_2, **b**, SnS_2 and **c**, $Sn(S_{0.92}Se_{0.08})_2$ ETLs, respectively.

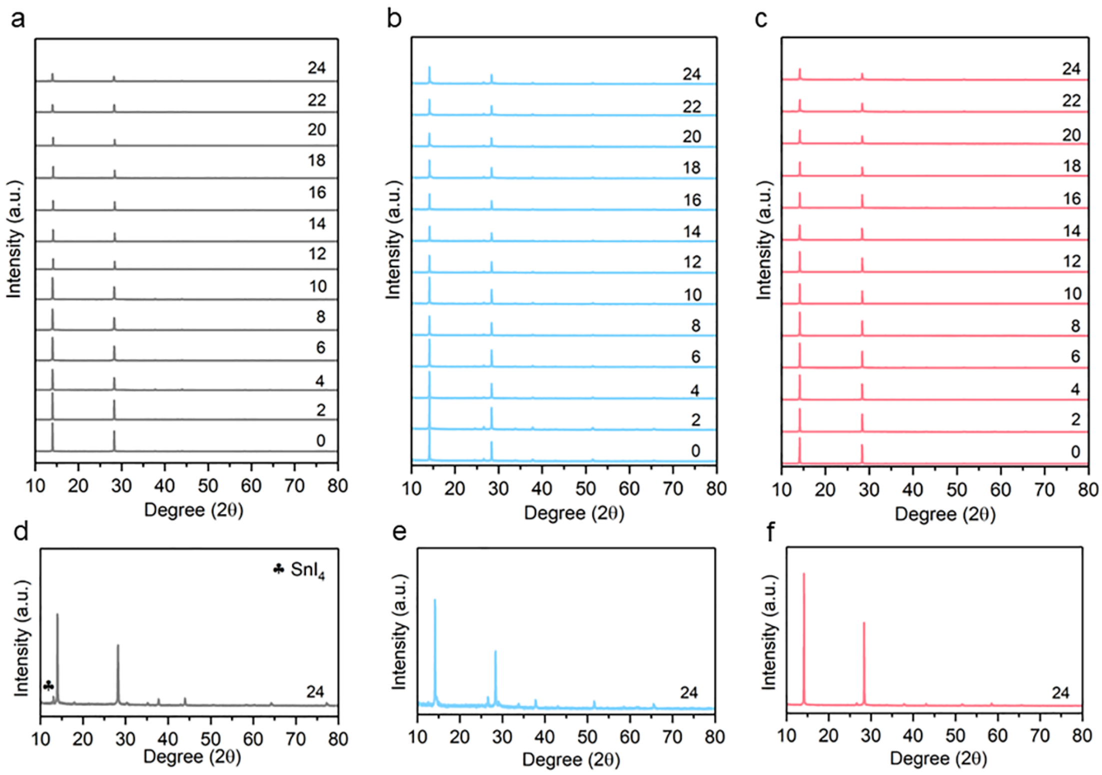

Supplementary Fig. 25. XRD patterns. XRD patterns of Sn-based perovskite layers gown on **a**, TiO_2, **b**, SnS_2 and **c**, $Sn(S_{0.92}Se_{0.08})_2$ ETLs after aging a period of time in air. The XRD patterns of Sn-based perovskite layers gown on **d**, TiO_2, **e**, SnS_2 and **f**, $Sn(S_{0.92}Se_{0.08})_2$ ETLs after aging for 24 days were plotted individually.

Supplementary Table 1. Photovoltaic parameter comparison of this work and existing *nip*-type TPSCs.

Devices	V_{OC} (V)	J_{SC} (mA cm^{-2})	FF (%)	PCE (%)	Stability/Condition	Year	Ref
FTO/Se-SnS_2/ $PEA_{0.15}FA_{0.85}SnI_{2.85}Br_{0.15}$-AET/PTAA/Ag	**0.73**	**22.28**	**72.68**	**11.78**	**Maintaining 95% of its initial PCE for 1600 h/in a N_2 glovebox**		
FTO/c-TiO_2/mp- TiO_2/$MASnI_3$/Spiro-OMeTAD/Au	0.88	16.80	42.00	6.40	—	2014	1
FTO/bl-TiO_2/mp- TiO_2/$MASnI_3$/Spiro-OMeTAD/Au	0.68	16.30	48.00	5.23	Maintaining 64% of its initial PCE for 24 h/in a N_2 glovebox	2014	2
FTO/c-TiO_2/mp-TiO_2/$CsSnI_3$+SnF_2/HTM/Au	0.24	22.70	37.00	2.02	—	2014	3
FTO/bl-TiO_2/mp-TiO_2/$FASnI_3$+SnF_2/spiro-OMeTAD/Au	0.24	24.45	36.00	2.10	—	2015	4
FTO/bl-TiO_2/mp- TiO_2/$MASnI_3$/Au	0.32	21.40	46.00	3.15	—	2015	5
FTO/bl-TiO_2/mp-TiO_2/$FASnI_3$+SnF_2+Pyrazine/spiro-OMeTAD/Au	0.32	23.70	63.00	4.80	Maintaining 98% of its initial PCE for 100 days/with encapsulation	2016	6
FTO/TiO_2/Al_2O_3/$CsSnIBr_2$+SnF_2+HPA/Carbon	0.31	17.40	57.00	3.20	No significant decay for 77 days/with encapsulation	2016	7
FTO/c-TiO_2/mp-TiO_2/$CsSnBr_3$+N_2H_4/PTAA/Au	0.38	19.92	51.73	3.89	—	2017	8
FTO/bl-TiO_2/mp-TiO_2/$BA_2MA_3Sn_4I_{13}$ +TEP/PTAA/Au	0.23	24.10	45.7	2.53	Maintaining 90% of its initial PCE for 30 days/with encapsulation	2017	9
FTO/c-TiO_2/mp-TiO_2/{en}$FASnI_3$/PTAA/Au	0.48	22.54	65.96	7.14	Maintaining 96% of its initial PCE for 1000 h/with encapsulation	2017	10
FTO/c-TiO_2/mp-TiO_2/{en}$MASnI_3$/PTAA/Au	0.43	24.28	63.72	6.63	Maintaining ~60% of its initial efficiency for 10 min/constant illumination in air	2017	11
FTO/c-TiO_2/mp-TiO_2/$MASnIBr_2$+SnF_2/spiro-OMeTAD/Au	0.45	13.77	59.58	3.70	Maintaining 80% of its initial PCE for 60 days/in a N_2 glovebox	2018	12
FTO/TiO_2/$HEA_{0.4}FA_{0.6}Sn_{0.67}I_{2.33}$/Carbon	0.37	18.52	56.20	3.90	No significant decay for 100 h/in a N_2 glovebox	2018	13
ITO/nanoporous TiO_2 ZrO_2/carbon/ (4AMP) $(FA)_3Sn_4I_{13}$	0.64	14.90	44.30	4.22	Maintaining 91% of its initial PCE for 100 h/constant illumination in N_2 atmosphere at 45 °C	2018	14
FTO/ c-TiO_2/mp-TiO_2/$MASnI_3$ /PTAA/Au	0.49	22.91	64.00	7.13	—	2019	15
FTO/c-TiO_2/mp- TiO_2/{*en*}$FASnI_3$/BDT-4D/Au	0.497	22.41	68.21	7.59	—	2019	16
FTO/bl-TiO_2/mp-TiO_2/$BA_2(FA)_{n-1}Sn_nI_{3n+1}$/PTAA/Au	0.42	23.98	40.21	4.04	Maintaining 80% of its initial PCE for 14 days/in a N_2 glovebox	2020	17
FTO/c-TiO_2/mp-TiO_2/$CsSnI_3$+MBAA/P3HT/Ag	0.45	24.85	67	7.5	the average PCE of MBAA-modified devices maintained 60.2% of their original value after being stored under an inert RT condition for 1440 h	2021	18
FTO/bl-TiO_2/mp-TiO_2/$Cs_{0.1}FA_{0.9}SnI_3$+ThMAI/PTAA/Au	0.52	24.12	72.02	9.06	—	2021	19
FTO/bl-TiO_2/mp-TiO_2/$FASnI_3$/spiro-OMeTAD:DPI-TPFB/Au /Ag	0.649	23.59	71.25	10.9	The encapsulated device retained 86% of its initial PCE after storing for 2832 h at room temperature (RT) in the dark with a humidity level of ≈30%	2023	20

Supplementary Table 2. The VBMs, CBMs, and bandgaps of the perovksite film, TiO_2 ETL, SnS_2 ETL, and $Sn(S_{0.92}Se_{0.08})_2$ ETL, respectively.

	VBM (eV)	CBM (eV)	Bandgap (eV)
Perovskite	-5.14	-3.73	1.41
TiO_2	-7.23	-4.23	3.00
SnS_2	-6.62	-3.98	2.64
$Sn(S_{0.92}Se_{0.08})$	-6.43	-3.83	2.60

Supplementary Table 3. The conductivities and mobilities of TiO_2, SnS_2 and $Sn(S_{0.92}Se_{0.08})_2$ films, respectively.

Samples	TiO_2	SnS_2	8%-Se-SnS_2
Conductivity (S cm^{-1} x10^{-3})	8.41	12.7	13.8
Mobility (x10^{-3} $cm^2 v^{-1} s^{-1}$)	7.15	54.3	63.4

Supplementary Table 4. The fitted data of TRPL characterization.

Sample	TiO_2/Perovskite	SnS_2/Perovskite	$Sn(S_{0.92}Se_{0.08})_2$/Perovskite
τ_1 (ns)	8.32	6.65	3.51

Supplementary Table 5. Photovoltaic parameters of *nip*-type TPSCs based on TiO_2, SnS_2, and $Sn(S_xSe_y)_2$ (y = 3%, 5%, 7%, 8%, 9% and 10%, x+y=1), respectively.

Samples		V_{oc} (V)	J_{sc} (mA/cm^2)	FF (%)	Efficiency (%)
TiO_2	Best	0.48	20.47	71.11	6.98
	Average	0.42±0.06	21.21±0.72	67.96±2.80	6.03±0.86
SnS_2	Best	0.57	21.89	72.88	9.03
	Average	0.54±0.02	20.18±0.82	72.48±0.99	7.89±0.45
$Sn(S_{0.97}Se_{0.03})_2$	Best	0.61	20.12	74.45	9.17
	Average	0.59±0.02	20.24±0.33	72.58±1.29	8.72±0.39
$Sn(S_{0.95}Se_{0.05})_2$	Best	0.65	20.02	75.76	9.88
	Average	0.63±0.02	20.25±0.51	73.68±1.55	9.37±0.43
$Sn(S_{0.93}Se_{0.07})_2$	Best	0.68	20.43	76.52	10.58
	Average	0.66±0.02	20.33±0.29	73.93±1.55	9.98±0.49
$Sn(S_{0.92}Se_{0.08})_2$	Best	0.73	22.28	72.68	11.78
	Average	0.70±0.01	20.73±0.88	73.97±1.47	10.77±0.47
$Sn(S_{0.91}Se_{0.09})_2$	Best	0.73	22.25	71.54	11.60
	Average	0.70±0.02	20.35±0.71	73.14±1.85	10.45±0.56
$Sn(S_{0.90}Se_{0.10})_2$	Best	0.74	20.42	74.56	11.31
	Average	0.71±0.02	19.72±0.63	72.89±1.35	10.24±0.55

Supplementary References

1. Noel, N. K. et al. Lead-free organic-inorganic tin halide perovskites for photovoltaic applications. *Energy Environ. Sci.* **7,** 3061–3068 (2014).
2. Hao, F. et al. Lead-free solid-state organic-inorganic halide perovskite solar cells. *Nat. Photon.* **8,** 489–494 (2014).
3. Kumar, M. H. et al. Lead-free halide perovskite solar cells with high photocurrents realized through vacancy modulation. *Adv. Mater.* **26,** 7122–7127 (2014).
4. Koh, T. M. et al. Formamidinium tin-based perovskite with low Eg for photovoltaic applications. *J. Mater. Chem. A.* **3,** 14996–15000 (2015).
5. Hao, F. et al. Solvent-mediated crystallization of $CH_3NH_3SnI_3$ Films for heterojunction depleted perovskite solar cells. *J. Am. Chem. Soc.* **137,** 11445–11452 (2015).
6. Lee, S. J. et al. Fabrication of efficient formamidinium tin iodide perovskite solar cells through SnF_2–pyrazine complex. *J. Am. Chem. Soc.* **138,** 3974–3977 (2016).
7. Li, W. et al. Addictive-assisted construction of all-inorganic $CsSnIBr_2$ mesoscopic perovskite solar cells with superior thermal stability up to 473 K. *J. Mater. Chem. A.* **4,** 17104–17110 (2016).
8. Song, T. -B. et al. Importance of reducing vapor atmosphere in the fabrication of tin-based perovskite solar cells. *J. Am. Chem. Soc.* **139,** 836–842 (2017).
9. Cao, D. H. et al. Thin films and solar cells based on semiconducting two-dimensional Ruddlesden–Popper $(CH_3(CH_2)_3NH_3)_2(CH_3NH_3)_{n-1}SnnI_{3n+1}$ perovskites. *ACS Energy Lett.* **2,** 982–990 (2017).
10. Ke, W. et al. Enhanced photovoltaic performance and stability with a new type of hollow 3D perovskite {en}$FASnI_3$. S*ci. Adv.* **3,** e1701293 (2017).
11. Ke, W. et al. Efficient lead-free solar cells based on hollow {en}$MASnI_3$ perovskites. *J. Am. Chem. Soc.* **139,** 14800–14806 (2017).
12. Xiao, M. et al. Tin-based perovskite with improved coverage and crystallinity through tin-fluoride-assisted heterogeneous nucleation. *Adv. Optical Mater.* **6,** 1700615 (2018).
13. Tsai, C. -M. et al. Control of crystal structures and optical properties with hybrid formamidinium and 2-hydroxyethylammonium cations for mesoscopic carbon-electrode tin-based perovskite solar cells. *ACS Energy Lett.* **3,** 2077–2085 (2018).
14. Chen, M. et al. Lead-free Dion–Jacobson tin halide perovskites for photovoltaics. *ACS Energy Lett.* **4,** 276–277 (2019).
15. Li, F. et al. A cation-exchange approach for the fabrication of efficient methylammonium tin iodide perovskite solar cells. *Angew. Chem. Int. Ed.* **58,** 6688–6692 (2019).
16. Vegiraju, S. et al. Benzodithiophene hole-transporting materials for efficient tin-based perovskite solar cells., *Adv. Funct. Mater.* **29,** 1905393 (2019).
17. Li, F. et al. Effects of alkyl chain length on crystal growth and oxidation process of two-dimensional tin halide perovskites. *ACS Energy Lett.* **5,** 1422–1429 (2020).
18. Tao, Y. et al. Ambient-air-stable lead-free $CsSnI_3$ solar cells with greater than 7.5% efficiency., *J. Am. Chem. Soc.* **143,** 4319−4328 (2021)
19. Hu, M. et al. Regulating the surface passivation and residual strain in pure tin perovskite films. *ACS Energy Lett.* **6,** 3555−3562 (2021).
20. Hu, M. et al. Highly stable n–i–p structured formamidinium tin triiodide solar cells through the stabilization of surface Sn^{2+} cations. *Adv. Funct. Mater.* **33,** 2300693 (2023).